

Protokoll  
Neurobiologisches Großpraktikum

# **Color-blindness of direction-selective units in the zebrafish optic tectum**

**Alexander Wendt, Patrick Weygoldt**

Supervised by:

Tim Hladnik, David Burkardt, Aristides Arrenberg  
Systems Neurobiology  
Werner Reichardt Centre for Integrative Neuroscience  
Tuebingen University

February 26, 2023

# 1 Introduction

Sensory information about the environment is crucial for survival. Especially the sensory modality of light is essential to perceive the outside world in many vertebrates. In primates, the incoming light is absorbed by three photoreceptors, which enable color vision (Marc et al., 1977). Another visual feature processed by the same sensory modality are temporal changes such as the movement of objects. Whether these two features are processed separately and how they may still interact is strongly disputed (Gegenfurtner et al., 1996). Livingstone et al. (1988) argued, that the segregation of color and movement is facilitated by the pathway selectivity and differences in the encoding of "color selectivity, contrast sensitivity, temporal properties and spatial resolution" of cells in the geniculate. Cells that encode for color are in a separate pathway (parvocellular geniculate pathway, motion in magnocellular geniculate pathway) and have properties that ensure only color vision (Livingstone et al., 1988). This separation of pathways from color and motion implies that motion should only be perceivable if the visual display contains luminance contrasts (Mullen et al., 1992). In contrast to Livingstone, Mullen et al. (1992) used an isoluminant chromatic stimulus to demonstrate a connection between color and motion where the motion pathway received small amounts of chromatic information and vice versa. fMRI studies with human subjects imply that color vision is physiologically widely distributed, and not defined for only one pathway (Wandell et al., 1999). Motion perception can be subdivided into three orders of processing (Lu, Lesmes, et al., 1999). First-order motion is the percept of objects that are defined by their luminance and is derived from a "Hassenstein-Reichardt-Detector", which consists of two units that compare the luminance at two different spatial locations (Borst et al., 2011; Lu and Sperling, 2001). Whereas second-order motion is detecting motion stimuli that consist of equal luminance but differ in "contrast, spatial frequency, texture type, or flicker" (Lu and Sperling, 2001). Lastly, the third-order motion is defined as a figure relative to the background (Lu, Lesmes, et al., 1999). Lu, Lesmes, et al. (1999) proposed that isoluminant motion is computed by the third-order system, a brain region where "binocular inputs of form, color, depth, motion, and texture are all available" (Lu, Lesmes, et al., 1999).

From an evolutionary perspective, color vision in primates is a recent development (Yokoyama et al., 2001). This is not the case for zebrafish (Baden, 2021). To understand the physiological segregation of color- and motion perception, we explored the perception of the zebrafish (*Danio rerio*), a very basal vertebrate. In fish, color vision evolved independently from primates, providing a comparative approach (Daw, 1967).

## 1.1 Motion perception in zebrafish

Zebrafish presents the unique opportunity to combine whole-brain imaging data with behavior to complex visual stimuli (Bollmann, 2019). The retina of the zebrafish has a similar cell structure and pathways compared to mammalian retinas, making it comparable to human retinas (Bollmann, 2019). The visual system is developed early after fertilization, in a time-span of three days (Stuermer, 1988), and after the three days, zebrafish reliably respond to light (R.-w. Zhang et al., 2010). In addition to a comparable retina, zebrafish also exhibit the optokinetic response (OKR), a reflex also present in humans. The OKR describes then the movement of eyes in the direction of a moving stimulus, which is interrupted by rapid saccades in the opposite direction (Brokerhoff et al., 1995). The OKR is encoded in the velocity-to-position neural integrator (VPNI) which is located in the caudal hindbrain (Miri, Daie, Arrenberg, et al., 2011; Miri, Daie, Burdine, et al., 2011). Aside from the circuitry for the OKR, Perez-Schuster et al. (2016) results indicate that direction-selective tectal cells had a sustained rhythmic activity after stimulation that elicited the OKR. Wang, Hinz, Y. Zhang, et al. (2020) investigated receptive fields of the pretectum and tectum of motion-selective neurons. Neurons in the pretectum have large receptive fields for the lower

visual fields, whereas tectal neurons have mostly small receptive fields for the upper nasal visual field (Wang, Hinz, Y. Zhang, et al., 2020). This underlines the notion that motion-selective cells in the pretectum and tectum correspond to different functions. The pretectum is vital for the optomotor response (OMR), where fish swim in the direction of the optic flow, and the tectum for near-field prey capture (Wang, Hinz, Y. Zhang, et al., 2020 but see also Duchemin et al., 2022).

## 1.2 Color vision in zebrafish

Chromatic information, on the other hand, is first absorbed by the four photoreceptors with absorption peaks around 500 nm (red), 470 nm (green), 410 nm (blue), and 360 nm (UV) in the retina (Robinson et al., 1993). The photoreceptors are arranged in so-called "cone mosaics", and the ratios between photoreceptors in larval to adult zebrafish change (Allison et al., 2010). The position of the receptors has evolved to match the natural environment: In a natural scenery, there is hardly any color above the fish. Therefore the part of the retina that captures the light coming from above the fish consists is not specialized towards color vision (Zimmermann et al., 2018). The majority of chromatic information can is available below the fish up to its visual horizon, which is represented on the retina by an area rich in cones (Zimmermann et al., 2018). After the retina, visual stimuli are processed by the optic tectum, which is homologous to the superior colliculus, and also the pretectum and thalamus in the mammalian brain (Bollmann, 2019).

The segregation of color and motion on a behavioral level in zebrafish was demonstrated by Orger et al. (2005). Using a motion-nulling approach, they could show that the motion perception of zebrafish larvae relied on luminance contrast to perceive a moving stimulus (Chichilnisky et al., 1993). The physiological segregation of color and motion in the zebrafish brain is still unclear. The optic tectum is one of the first areas that receive retinal input (Bollmann, 2019), turning it into an ideal starting point to understand the physiological segregation that is reflected in the behavioral output during isoluminant chromatic motion stimulation. The question we tried to answer, was whether the tectal cells that show increases in their Calcium activity to directional motion still do so if the moving stimulus is isoluminant and the only motion cues are of chromatic nature. We investigated this question with a novel experimental setup, that can stimulate the fish globally with moving color gratings and simultaneously record the neural Calcium activity in the brain of zebrafish larvae as well as simultaneously quantify eye movements and swimming behavior.

## 2 Methods

### 2.1 Experimental animals

We used three transgenic zebrafish from Janelia farm with a good expression of Gcamp6 gen (*tg(HuC : GCamp6f)jf7*). For the experiments, the zebrafish were 5-6 days postfertilization (dpf) old. In two of the three, we recorded behavioral data.

### 2.2 Experimental setup

The stimulation arena consisted of a glass bulb that was coated in paint to be able to project light on it from the outside. The light was produced by a high power LED light source (CHROLIS-C1, Thorlabs Incorporated) and transmitted to a projector (DLP® LightCrafter™ 4500, Texas Instruments Incorporated) using a liquid light guide. The light exiting the projector was then reflected downwards in a 90° angle onto a square pyramidal mirror, that split the beam into four. Each of the four beams was then reflected by one of the four mirrors placed around the setup and consequently projected onto the glass sphere. The result is a spherical projection. The experimental setup is visualized in figure 1. The fish were embedded in Agarose on a custom designed stage that could be fixed inside the stimulus arena.

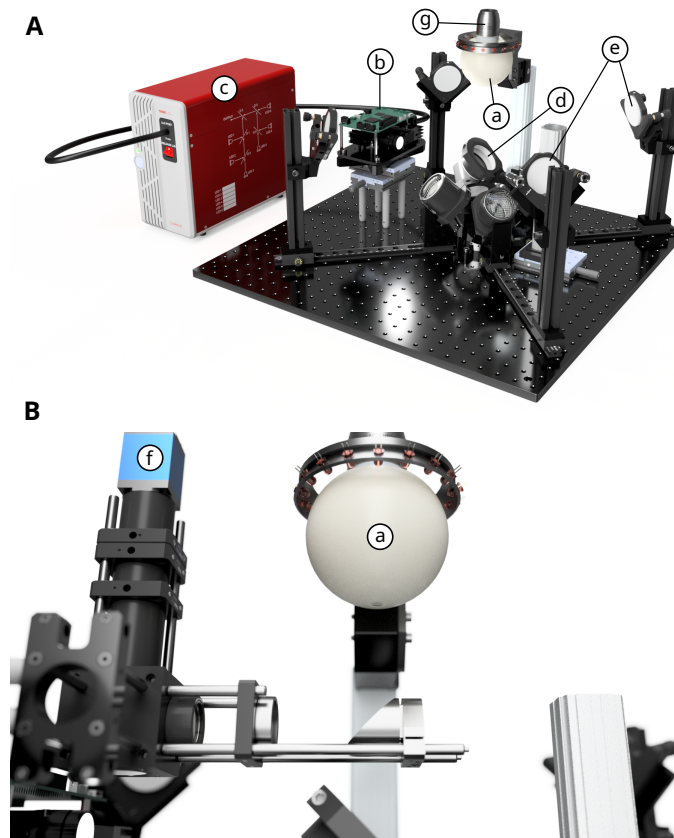


Figure 1 | **CAD rendering of the experimental setup.** **A** shows the whole recording setup excluding the camera recording behaviors of the fish. The fish is fixed inside a glass bulb (a) containing E3 medium. The light is produced by an LED light source (c), transferred to a projector (b) and projected onto a 45° mirror (d). The mirror reflects the projection onto a pyramid mirror (not visible in the current rendering), which splits the beam into four. The four beams are then reflected by four mirrors placed around the setup (e) and reflected onto the glass bulb from four sides. The result is a spherical projection into the glass bulb. The calcium activity was recorded by a moving objective microscope that peeks through an opening in the top of the glass sphere (g). **B** shows the camera (f) used to record through the bottom of the glass bulb using mirrors as well. Images are courtesy of Tim Hladnik.

### 2.2.1 Embedding procedure

The immobilization of the fish was conducted with 1,6 % low-melting Agarose, where it was submerged for a short time before a drop of Agarose containing the fish was placed on a Petri-dish to polymerize. Meanwhile, the plastic pipette was prepared (diagonal cut-off, see figure 2), placed on a 3D-printed stage, and filled with 2 % Agarose. After 30 min the stage was separated from the now polymerized Agarose. The immobilized fish was placed on the tip of the Agarose that stood out from the pipette tip. To combine the Agarose from the pipette and the Agarose where the fish was in, we added 1,6 % Agarose which filled the gap between those two Agarose blocks. The pipette was then inserted into a holding apparatus inside the glass sphere, which we filled with E3. For two of the three fish, we removed the Agarose around the eyes of the fish, so that the fish can move them (Figure 2).

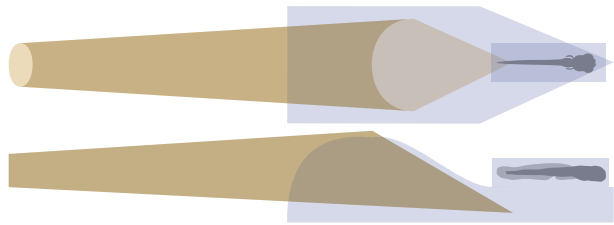


Figure 2 | **Agarose stage** to fixate the larvae. The stage consisted of a diagonal cut-off of a pipette tip (orange) and a small, pointed Agarose table (blue). The fish (gray) were separately embedded into a drop of Agarose. We pruned the edges and then placed the Agarose block containing the fish onto the point of the Agarose table.

### 2.2.2 Stimulus

The stimulus consisted of red and green gratings with six different logarithmically increasing contrast levels (0., 0.1, 0.18, 0.32, 0.56, 1.0) that were randomized. The stimulus time for one contrast level was 8 seconds long, divided into 4 seconds of no angular velocity and followed by 4 seconds with an angular velocity of  $30^{\circ} \text{ s}^{-1}$ . Two directions of velocity were used and they were randomized. This protocol was repeated 3 times and the order stayed the same across the repeats. Before the protocol started and after the protocol ended we implemented a pause with no stimulus for 15 seconds. The stimulus was generated using vxPY (<https://github.com/thladnik/vxPy>). The color contrast levels of the stimulus we displayed for this experiment were not yet linearised and which contrast levels the fish exactly perceived are unknown.

### 2.2.3 Calcium imaging

Calcium imaging was conducted with an infrared laser (Coherent Vision-S Ti-Sa laser, and a 25 x objective (Nikon CFI75, Tokyo, Japan), a wavelength of 920 nm), with a movable objective microscope (MOM) (Sutter Instruments, Novato, CA, USA). The resolution of the calcium imaging was 2 Hz. Before beginning the imaging protocol we checked if the fish was drifting out of the focal plane. For this procedure, we took a reference image and waited for 30 min, after that time we retook the image, compared it with our reference image and decided to start our stimulus protocol or to wait another 30 min. Calcium imaging was done in  $10 \mu\text{m}$  intervals along the optical axis. After each recording, we visually assessed the drift of the Agarose. If drifting occurred, we did not consider these recordings for the data analysis. For our three fish, we used 12, 5, and 5 recordings. For processing the Calcium-imaging data, we used suite2p, an open-source pipeline for processing two-photon calcium imaging data (Pachitariu et al., 2017).

### 2.2.4 Behavioral response

For a behavioral measure of the sensitivity to isoluminant chromatic motion stimuli, we chose the optokinetic response (OKR). Eye movements were recorded via a camera that recorded the bottom of the larva

through a 45° mirror below the glass bulb (see figure 1). A small area on the bottom of the bulb was not coated in paint and thus enabled a clear view into the underside of the fish. Image segmentation and eye tracking happened in real-time using vxPy (<https://github.com/thladnik/vxPy>). Eye velocities were recorded in degrees per second at a rate of 20 Hz.

## 2.3 Data analysis

We wrote our data analysis pipeline in Python 3.10.9 using the packages Numpy (Harris et al., 2020), Scipy (Virtanen et al., 2020), Matplotlib (Hunter, 2007), vxPy (<https://github.com/thladnik/vxPy>) and suite2p (Pachitariu et al., 2017). All scripts used for the analysis and plotting are publically available in a git repository.

### 2.3.1 Calcium data

First, we computed the  $\text{dff}$  of the fluorescence signal of every single ROI by formula 1.

$$\text{dff}(t) = \frac{f_{ROI}(t) - \langle f_{ROI}(t) \rangle}{\langle f_{ROI}(t) \rangle} \quad (1)$$

Where the difference between the fluorescence of a single point in time  $f_{ROI}(t)$  and the mean of the signal over time is divided by the mean. We further used the  $\text{dff}$  to compute the Z-score to quantify calcium activity (equation 2).

$$Z = \frac{\text{dff}(t) - \langle \text{dff}(t) \rangle}{\sigma_{\text{dff}(t)}} \quad (2)$$

The Z-score indicates how many standard deviations a certain point in time deviates from the mean of the signal, in this case, the  $\text{dff}$  of the signal. This is particularly useful in this context because peaks that originate from noise (in signals with a large standard deviation) are scaled down relative to peaks with a good signal-to-noise ratio. To simplify the analysis of multiple time series with different sampling rates, we computed for every separate stimulation phase the mean of the z-score and  $\text{dff}$ . This was possible because the sampling rate of the microscope was relatively low (2 Hz) and the stimulation phases were short. Taking the means significantly simplified the analysis while resulting in a minor loss of temporal resolution.

Since we targeted specifically direction selective cells, we constructed a data filtering pipeline that only provides the ROIs that respond to movements in a certain direction. In a first filtering step we excluded all individuals that did not respond to the stimulus. To do so, we computed the Spearman correlations between the z-scores of the same ROI across the three identical repeats of the stimulation. This resulted in three correlation coefficients per ROI, from which we then took the mean. To choose the units with the strongest auto-correlation, we estimated the distribution of the resulting correlation coefficients by a convolution with a Gaussian kernel. We then chose the ROIs that fell into a 20% integral of the right tail of the distribution (Figure 3).

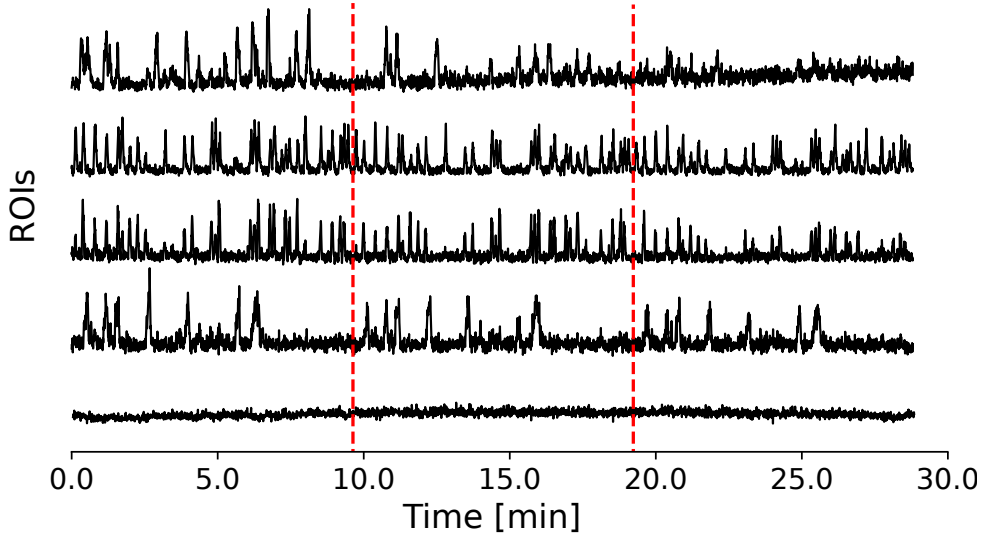


Figure 3 | **Calcium signal (Z-score) over time** from various ROIs. Red lines indicate the three repetitions.

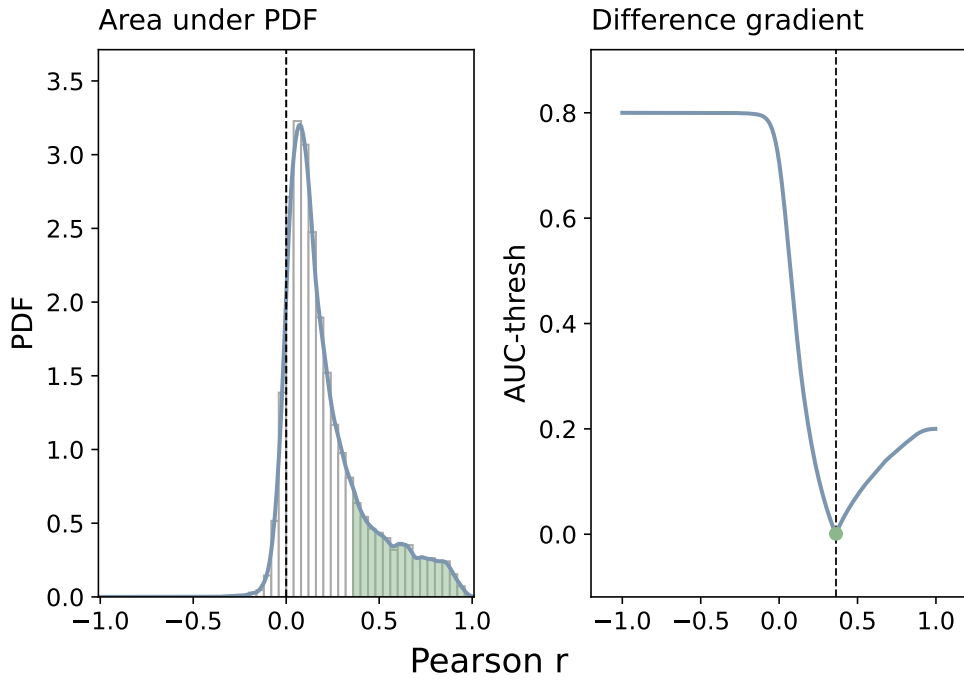
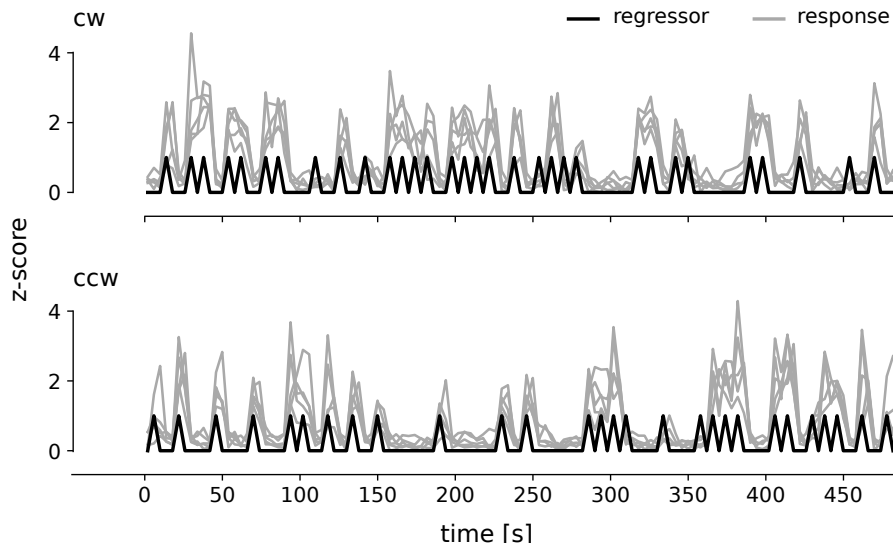


Figure 4 | **Probability density of autocorrelations.** **Left:** Probability density function of the mean correlation coefficients computed between the stimulation repeats of a single ROI. The green tail indicates the area that was chosen to include the ‘active’ ROIs, i.e. the ones that were correlated strongly between the trials, which indicates repeatable response to the stimulus. **Right:** Difference gradient that was used to obtain all ROIs that fall into the green area. To obtain this, we computed the area under the curve (AUC) between the one and an array of index values and then subtracted it from our target AUC of 0.2.

In a next filtering step, we had to select all ROIs that responded specifically to either clockwise or counterclockwise motion. To do so, we created motion regressors for either direction and correlated them with the z-scores. All ROIs that crossed the correlation threshold of 0.2 were included in the analysis. Figure 5 shows an example of some z-scores and the regressors. In a next step, we removed all stimulus phases where no motion stimulus was presented and then computed the means and standard deviations for each stimulus categories for all fish and all repeats for a single fish.



**Figure 5 | Motion-direction regressors and correlated z-scores.** The black line show the regressors for clockwise (cw, top) and counterclockwise (ccw, bottom) respectively. The gray lines indicate the z-scores of some ROIs that were strongly correlated with the respective regressors.

### 2.3.2 Behavioral data

As a behavioral measure we chose the eye velocities. To make the velocities comparable across the stimulus categories we removed saccades in the signal by a median filter with a width of 41 data points. As in the calcium signal, we then computed the mean eye velocity for each stimulus phase. The second step of abstraction was to compute the means and standard deviations across stimulus repeats and across the two individuals we recorded behavioral data for.

### 3 Results

#### 3.1 Direction selective units in the optic tectum

In total, we recorded 14371 units in the optic tectum of 3 zebrafish larvae (Figure 6). Our preprocessing pipeline extracted 129 units to be distinctly direction selective for either ccw or cw movement. Figure 6 serves as an overview of the data set after it passed our preprocessing pipeline. The shade of the heatmap encodes the z-score of the respective ROI in the respective stimulus phase. It also illustrates the raw data, i.e. in the recorded temporal resolution instead of the means per phase. The bar on top illustrates single stimulus phases by a green and a red bar. The contrast levels for green and red were linearized for visualization purposes. Data in figure 6 is visualized excluding the pauses of stimulation. Additionally, the previously randomized stimulation phases (motion direction and contrast levels) are now sorted. The left side shows the ccw moving stimulus phases and the right side the cw moving phases. On each side, all levels of green contrast are sorted by their combination with red contrast. The lowest row of the heatmap includes a subset of the units we excluded from our analysis. The second line from the bottom illustrates a subset of units that were considered to be 'active', i.e. showed auto-correlations that crossed our threshold. The two rows above show the complete dataset that passed the filtering steps and was included in the analysis. These rows nicely illustrate that the direction selective units we picked from the dataset using the regressor-correlation only show activity for their respective rotation direction. If we consider the chromatic stimulus levels, the same pattern appears in both populations: For stimuli with strong achromatic contrast, i.e. where red contrast is zero and green contrast increases (left sides of ccw and cw columns), the recorded calcium activity increases with increasing luminance contrast. If we consider the right side of the stimulus column for both populations, i.e. where red contrast is strongest and green contrast increases, we see the opposite pattern: While the luminance contrast is high, calcium activity is strong. But as the stimulus approaches isoluminance, i.e. chromatic contrast becomes the main driver of the response, calcium activity decreases.

In figure 7 we only included direction selective units and computed the mean and standard deviations for every stimulus phase across all individuals, ROIs, and repeats. The resulting data is plotted as a line plot for the combination of every single possible level of green contrast separately combined with all possible combinations of red contrast (figure 7, (B)). This is the same order that we chose to visualize the stimulus in figure 6. If the units we recorded did not respond to isoluminant chromatic contrasts, the line plots should show a trough where the red and green contrast is the same. This point is denoted by a dashed vertical line. For a green contrast level of 0 the minimum for both cw and ccw line plots is at 0. This is to be expected since motion is not supposed to be encodable if there is neither luminance nor chromatic cues that make it perceivable. For the green contrast levels of 0.1 and 0.18 however, the minima are both just right of the dashed vertical line. This indicates firstly, that a isoluminant chromatic contrast evokes the lowest response in direction selective units and secondly, that the green channel was perceived stronger than the red channel by the fish. The same pattern is observable for a green contrast of 0.32. For green contrast levels above that no trough is visible.

In figure 7, (C) top, we visualized all possible stimulus combinations in the same way we visualized the mean z-scores from (B): All possible levels of green are plotted in the columns of the matrix and all possible levels of red contrast are plotted in the rows of the matrix. The luminance contrast increases strongest along the x- and y-dimension of the matrix, while the isoluminant, chromatic contrast increases along the diagonal of the matrix. Below that we then visualized the average z-scores that are already plotted in (B) in the same way. The resulting heat map shows an increase in the z-scores along the x-

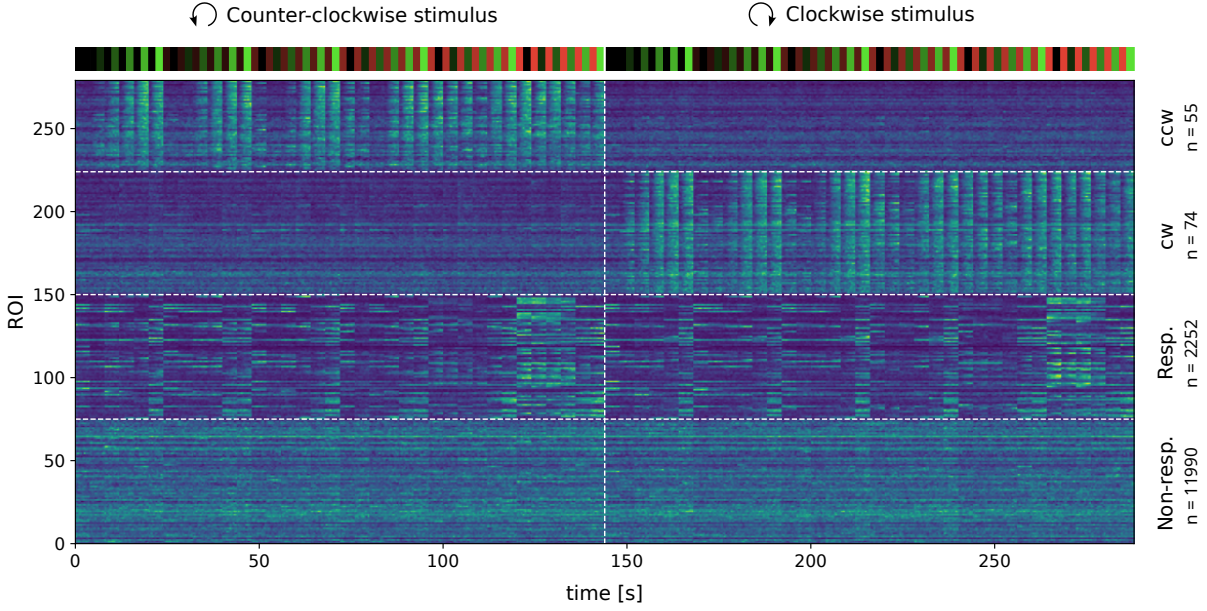


**Figure 6 | Overview of selected ROIs** after they passed through our preprocessing pipeline. As opposed to our stimulus protocol, the data is sorted according to rotation direction and contrast levels. Data is plotted for just the first of three stimulus repetitions. Units in the lowest category show now apparent pattern of activity in response to the stimulus. Units that are considered to be just responsive but not direction selective show a pattern that corresponds to the stimulus but does not change between the two rotation directions. Unit that were selected to be direction selective only show an activity pattern that corresponds to the stimulus in their respective rotation direction.

and y-axes, i.e. where luminance contrast increases. The diagonal, where the stimulus was assumed to be isoluminant and consisting of exclusively chromatic contrast, the heat map has a local minimum. This shows, that stimuli with more chromatic contrast than luminance contrasts resulted in lower activity in the direction selective neurons of the optic tectum. In addition, the heat map shows stronger activation along the x-axis (green contrast increase) compared to the y-axis (red contrast increase). This, in combination with the notion that the diagonal of inactivity is shifted towards the red channel, supports the assumption that the green channel was perceived stronger by the fish.

### 3.2 Optokinetic response

Figure 8 shows the recorded eye velocities in a similar manner as the calcium data visualized in figure 7. Panel (B) shows the mean eye velocities in all stimulus phases computed across both subjects and all stimulus repeats. Each subplot illustrates a single level of green contrast in combination with all possible levels of red contrast. If the driver of the observed behavior was luminance more than chromaticity, we should again see a trough in the mean eye velocity where the levels of green and red contrasts were the same, i.e. at the dashed vertical lines. As in figure 7, the trough approximately follows the dashed vertical line through the subplots. Again, the same pattern is observable in panel C of figure 8. The diagonal includes the lowest mean eye velocities, suggesting that the behavioral response was mainly driven by the luminance, instead of chromaticity. As in figure 7 (C), the diagonal is slightly shifted upwards. This further strengthens our assumption, that the green channel was perceived with a higher intensity.

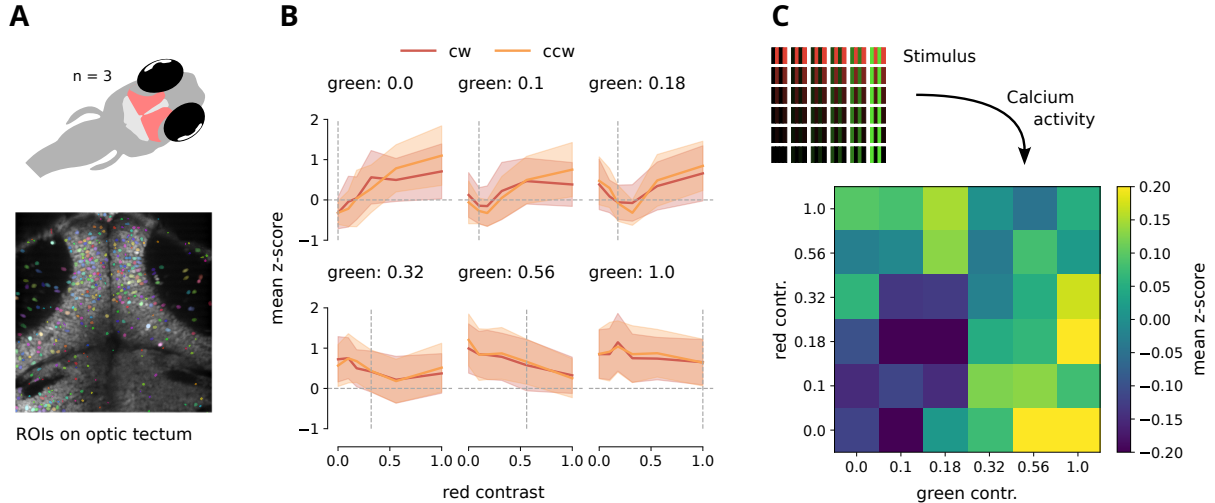


**Figure 7 | Calcium activity for different contrast levels.** (A) Location of the optic tectum in the brain of a zebrafish embryo. The lower figure illustrates the regions of interest in the optic tectum for which the activity was measured. (B) The mean z-score in all active units for ccw (orange) and cw (red) direction selective units. Each subplot shows the mean and standard deviation for one distinct level of green contrast in comparison to all possible combination of red contrast for this respective green level. The dashed vertical line denotes the value on the x-axis for which only color contrast was expected to drive a response. Thus we expect troughs in activity at the positions of the dashed line. (C) Shows the different levels of the stimulus contrast illustrated in a matrix where red contrast decreases in each row and green contrast increases in each column. The heat map below illustrates the mean z-score pooled for both rotation directions organized in the same way as the stimulus matrix. If given the assumption that red and green contrast was perceived equally and that color contrast alone does not drive the activity of motion direction selective units, we expected diagonal with low z-scores.

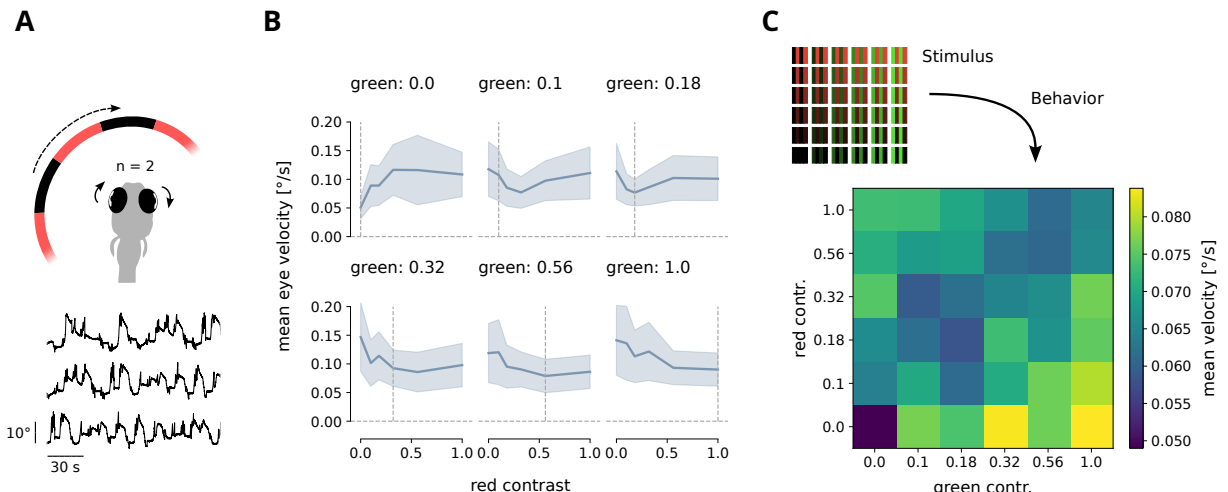


**Figure 8 | Behavioral responses to different contrast levels.** (A) Illustration of stimulus presentation and saccadic measurements to quantify the optokinetic response. (B) Mean and standard deviation of eye velocity for every level of green contrast (each subplot) as a function of all possible corresponding red contrast levels. The dashed vertical line illustrates the point in which, given that contrasts are perceived equally, only chromatic contrast should govern the behavioral response. If fish did not respond to exclusively color contrasts, the trough of the mean line should follow this point on the x-axis. (C) Stimulus and behavioral results quantified in the mean eye velocity are plotted in the same way as described in figure 7. If the chromatic contrast did not contribute to the behavioral response, we would expect a diagonal of decreased eye velocity.

## 4 Discussion

Our preprocessing pipeline successfully separated the direction-selective units from the population in the optic tectum. All units we analyzed were only active in their respective assigned motion direction despite the relatively low threshold we used to select them, as shown in figure 6. These direction selective cells showed the lowest activity to isoluminant chromatic contrasts. The eye velocities also show this decrease, albeit not as strong as the cellular response.

### 4.1 Direction selective cells in the optic tectum may be colorblind

We found a decreased response, both on the level of the calcium activity of direction-selective tectal units - and behavior when the stimulus shifted from achromatic motion cues towards chromatic motion cues. This suggests that chromatic information is used less or not at all to encode motion direction in the optic tectum. The lack of a true zero cline and the fact that the response on the diagonal of the heatmap (figure 7) still increases with increasing chromatic contrast between the stripes can be interpreted in two different ways regarding the implementation of the current version of this experiment. The first interpretation could be, that there is in fact a true zero cline on the diagonal, but the stimulus levels we used were not diverse enough to target this region. If the stimulus is never truly isoluminant, a small amount of luminance contrast would still be able to stimulate the units. This luminance contrast would not increase with the intensity of both channels, however, the overall contrast sensitivity of the visual system is dependent on light intensity. This would also explain why the response to (seemingly) isoluminant chromatic contrasts increases, as the (not purely) chromatic contrasts increase. To test this hypothesis, a stimulation setup with increased precision in its tunability would be needed. In addition to that, one would need to increase the levels of contrasts that are presented. However, since all possible combinations of contrasts are presented, the number of stimulus phases needed would increase quadratically, making this approach less realistic. The second interpretation could be, that luminance may be the primary cue that is used for motion processing, but the optic tectum receives integrated information from the retina, which contains some color information. To our knowledge, there is no data on chromatic inputs into the optic tectum that interact with motion encoding circuits (Robles et al., 2014; Wang, Hinz, Y. Zhang, et al., 2020).

For further studies, one could use color gratings moving in more directions than only the horizontal plane. For the zebrafish were three subtypes of direction-selective cells identified that can be used for a more robust dataset (Nikolaou et al., 2012). Another suggestion can be the combination of color gratings in an optic flow stimulus, to have more natural stimuli.

### 4.2 The behavioral response is not as strong as the physiological response

The main factor that explains elevated eye velocities, even for invisible stimuli, is our analysis pipeline. Since eye velocities are given in degrees per second, one of the stimuli will always result in negative velocities. To deal with this, we took the absolute velocities of both signals. The result is, that noise in the velocity signal that jitters around zero, and hence has a mean of approximately 0, becomes positive, with a mean above zero. This makes it hard to compare the two heatmaps in figure 7 and figure 8 quantitatively. To improve on this, a future iteration of our analysis pipeline should simply switch the sign of the signal depending on the motion direction of the stimulus. This would keep the mean of noisy data around 0, while still making the velocities across the stimulus categories comparable.

However if after this change in the pipeline, we observe the same pattern, it could be interpreted in multiple

ways. The behavioral zero-cline on the heatmap of figure 8 is not as prominent as the same figure for the calcium data in figure 7. A first possible explanation could be a direct consequence of the interpretation, that a small amount of chromatic information might still be able to contribute to motion perception. In fact, more chromatic information could be integrated in areas downstream of the optic tectum, resulting in a higher behavioral sensitivity to moving chromatic cues compared to the physiological level in the optic tectum. Another explanation could be, that in contrast to Orger et al. (2005) we used the OKR, which could make a difference in the response to an isoluminant stimulus. But this would imply that the OKR and the OMR differ in how chromatic information is indicated in the behavioral output while at the same time sharing components in the pretectum and both encoding similar large-field motion stimuli (Bollmann, 2019; Wang, Hinz, Haikala, et al., 2019). Another, perhaps easier explanation could be, that behavioral measurements are inherently noisier than measurements of neural activity. In the end, the change in the preprocessing pipeline combined with a strongly increased sampling size should suffice to explain and perhaps completely resolve this discrepancy.

### 4.3 Summary

In conclusion, we found an indication that motion and color are processed separately in the zebrafish optic tectum and that the motion processing pathway only includes achromatic information. For the first time, we show that this may be reflected on a physiological level in the optic tectum. Additionally, we see the same pattern manifested in the behavioral output.

## References

- Allison, W Ted et al. (2010). "Ontogeny of cone photoreceptor mosaics in zebrafish". In: *Journal of Comparative Neurology* 518.20, pp. 4182–4195.
- Baden, Tom (2021). "Circuit mechanisms for colour vision in zebrafish". In: *Current Biology* 31.12, R807–R820. issn: 0960-9822. doi: <https://doi.org/10.1016/j.cub.2021.04.053>.
- Bollmann, Johann H. (Sept. 15, 2019). "The Zebrafish Visual System: From Circuits to Behavior". In: *Annual Review of Vision Science* 5.1, pp. 269–293. issn: 2374-4642, 2374-4650. doi: [10.1146/annurev-vision-091718-014723](https://doi.org/10.1146/annurev-vision-091718-014723).
- Borst, Alexander et al. (2011). "Seeing Things in Motion: Models, Circuits, and Mechanisms". In: *Neuron* 71.6, pp. 974–994. issn: 0896-6273. doi: <https://doi.org/10.1016/j.neuron.2011.08.031>.
- Brokerhoff, Susan E et al. (1995). "A behavioral screen for isolating zebrafish mutants with visual system defects." In: *Proceedings of the National Academy of Sciences* 92.23, pp. 10545–10549.
- Chichilnisky, Eduardo-José et al. (Oct. 1993). "Functional Segregation of Color and Motion Perception Examined in Motion Nulling". In: *Vision Research* 33.15, pp. 2113–2125. issn: 00426989. doi: [10.1016/0042-6989\(93\)90010-T](https://doi.org/10.1016/0042-6989(93)90010-T).
- Daw, Nigel W. (1967). "Goldfish Retina: Organization for Simultaneous Color Contrast". In: *Science* 158.3803, pp. 942–944. doi: [10.1126/science.158.3803.942](https://doi.org/10.1126/science.158.3803.942).
- Duchemin, Auriane et al. (2022). "Fourier Motion Processing in the Optic Tectum and Pretectum of the Zebrafish Larva". In: *Frontiers in Neural Circuits* 15. issn: 1662-5110. doi: [10.3389/fncir.2021.814128](https://doi.org/10.3389/fncir.2021.814128).
- Gegenfurtner, Karl R. et al. (1996). "Interaction of motion and color in the visual pathways". In: *Trends in Neurosciences* 19.9, pp. 394–401. issn: 0166-2236. doi: [https://doi.org/10.1016/S0166-2236\(96\)10036-9](https://doi.org/10.1016/S0166-2236(96)10036-9).
- Harris, Charles R. et al. (Sept. 2020). "Array programming with NumPy". In: *Nature* 585.7825, pp. 357–362. doi: [10.1038/s41586-020-2649-2](https://doi.org/10.1038/s41586-020-2649-2).
- Hunter, J. D. (2007). "Matplotlib: A 2D graphics environment". In: *Computing in Science & Engineering* 9.3, pp. 90–95. doi: [10.1109/MCSE.2007.55](https://doi.org/10.1109/MCSE.2007.55).
- Livingstone, Margaret et al. (1988). "Segregation of Form, Color, Movement, and Depth: Anatomy, Physiology, and Perception". In: *Science* 240.4853, pp. 740–749. doi: [10.1126/science.3283936](https://doi.org/10.1126/science.3283936).
- Lu, Zhong-Lin, Luis A. Lesmes, et al. (1999). "The mechanism of isoluminant chromatic motion perception". In: *Proceedings of the National Academy of Sciences* 96.14, pp. 8289–8294. doi: [10.1073/pnas.96.14.8289](https://doi.org/10.1073/pnas.96.14.8289).
- Lu, Zhong-Lin and George Sperling (Sept. 2001). "Three-systems theory of human visual motion perception: review and update". In: *J. Opt. Soc. Am. A* 18.9, pp. 2331–2370. doi: [10.1364/JOSAA.18.002331](https://doi.org/10.1364/JOSAA.18.002331).
- Marc, Robert E. et al. (1977). "Chromatic Organization of Primate Cones". In: *Science* 196.4288, pp. 454–456. doi: [10.1126/science.403607](https://doi.org/10.1126/science.403607).
- Miri, Andrew, Kayvon Daie, Aristides B Arrenberg, et al. (2011). "Spatial gradients and multidimensional dynamics in a neural integrator circuit". In: *Nature neuroscience* 14.9, pp. 1150–1159.

- Miri, Andrew, Kayvon Daie, Rebecca D Burdine, et al. (2011). "Regression-based identification of behavior-encoding neurons during large-scale optical imaging of neural activity at cellular resolution". In: *Journal of neurophysiology* 105.2, pp. 964–980.
- Mullen, K.T. et al. (1992). "Absence of smooth motion perception in color vision". In: *Vision Research* 32.3, pp. 483–488. ISSN: 0042-6989. DOI: [https://doi.org/10.1016/0042-6989\(92\)90240-J](https://doi.org/10.1016/0042-6989(92)90240-J).
- Nikolaou, Nikolas et al. (2012). "Parametric functional maps of visual inputs to the tectum". In: *Neuron* 76.2, pp. 317–324.
- Orger, Michael B. et al. (May 2005). "Channeling of Red and Green Cone Inputs to the Zebrafish Optomotor Response". In: *Visual Neuroscience* 22.3, pp. 275–281. ISSN: 0952-5238, 1469-8714. DOI: [10.1017/S0952523805223039](https://doi.org/10.1017/S0952523805223039).
- Pachitariu, Marius et al. (2017). "Suite2p: beyond 10,000 neurons with standard two-photon microscopy". In: *bioRxiv*. DOI: [10.1101/061507](https://doi.org/10.1101/061507).
- Perez-Schuster, Veronica et al. (2016). "Sustained rhythmic brain activity underlies visual motion perception in zebrafish". In: *Cell reports* 17.4, pp. 1098–1112.
- Robinson, Judith et al. (1993). "Zebrafish ultraviolet visual pigment: absorption spectrum, sequence, and localization." In: *Proceedings of the National Academy of Sciences* 90.13, pp. 6009–6012.
- Robles, Estuardo et al. (2014). "The Retinal Projectome Reveals Brain-Area-Specific Visual Representations Generated by Ganglion Cell Diversity". In: *Current Biology* 24.18, pp. 2085–2096. ISSN: 0960-9822. DOI: <https://doi.org/10.1016/j.cub.2014.07.080>.
- Stuermer, CA (1988). "Retinotopic organization of the developing retinotectal projection in the zebrafish embryo". In: *Journal of Neuroscience* 8.12, pp. 4513–4530.
- Virnstein, Pauli et al. (2020). "SciPy 1.0: Fundamental Algorithms for Scientific Computing in Python". In: *Nature Methods* 17, pp. 261–272. DOI: [10.1038/s41592-019-0686-2](https://doi.org/10.1038/s41592-019-0686-2).
- Wandell, Brian A et al. (1999). "Color Signals in Human Motion-Selective Cortex". In: *Neuron* 24.4, pp. 901–909. ISSN: 0896-6273. DOI: [https://doi.org/10.1016/S0896-6273\(00\)81037-5](https://doi.org/10.1016/S0896-6273(00)81037-5).
- Wang, Kun, Julian Hinz, Väinö Haikala, et al. (2019). "Selective processing of all rotational and translational optic flow directions in the zebrafish pretectum and tectum". In: *BMC biology* 17.1, pp. 1–18.
- Wang, Kun, Julian Hinz, Yue Zhang, et al. (Jan. 2020). "Parallel Channels for Motion Feature Extraction in the Pretectum and Tectum of Larval Zebrafish". In: *Cell Reports* 30.2, 442–453.e6. ISSN: 22111247. DOI: [10.1016/j.celrep.2019.12.031](https://doi.org/10.1016/j.celrep.2019.12.031).
- Yokoyama, Shozo et al. (Aug. 2001). "The Molecular Genetics and Evolution of Red and Green Color Vision in Vertebrates". In: *Genetics* 158.4, pp. 1697–1710. ISSN: 1943-2631. DOI: [10.1093/genetics/158.4.1697](https://doi.org/10.1093/genetics/158.4.1697).
- Zhang, Rong-wei et al. (2010). "Development of light response and GABAergic excitation-to-inhibition switch in zebrafish retinal ganglion cells". In: *The Journal of physiology* 588.14, pp. 2557–2569.
- Zimmermann, Maxime J.Y. et al. (July 2018). "Zebrafish Differentially Process Color across Visual Space to Match Natural Scenes". In: *Current Biology* 28.13, 2018–2032.e5. ISSN: 09609822. DOI: [10.1016/j.cub.2018.04.075](https://doi.org/10.1016/j.cub.2018.04.075).